Mechano-elastic and image modelling of strongyle larvae parasites of domestic animals

C. Papaodysseus, *Member, IEEE*, P. Rousopoulos, *Member, IEEE*, D. Dafi, *Member, IEEE*, M. Panagopoulos, *Member, IEEE*, V. Loumos, *Member, IEEE*, G. Theodoropoulos

***Abstract*— In this paper a novel methodology is introduced for obtaining the mechano-elastic properties of the third stage larvae of domestic animals' parasites. The introduced methodology incorporates elements of elastic beam theory, image processing, curve fitting and numerical analysis to evaluate the undeformed shape of a parasite given a digital image of a random parasite deformation. It is demonstrated that different orientations and deformations of the same parasite give rise to practically the same undeformed shape when the methodology is applied to the corresponding images, thus confirming the consistency of the approach. A preliminary analysis of the obtained results indicates that various characteristics of the computed undeformed shapes may be employed for automatic third stage larva identification from an image of parasite in an arbitrary deformed shape. Apart from being important from a medical point of view, knowledge of the mechano-elastic properties of third stage larvae may form the basis of a system for the automated classification of these parasites. The methodology introduced here offers a consistent quantization and exact evaluation of the mechano-elastic properties of these parasites and it manifests the characteristics that are deformation invariant.**

I. Introduction

One of the main ailments of the livestock industry is related to the threat of strongyles, which are common endoparasitic nematodes of domestic animals.

C. Papaodysseus is with the National Technical University of Athens, School of Electrical & Computer Engineering, Multimedia Technology Laboratory, Zographou Campus, 15773 Athens, Greece, (e-mail: cpapaod@cs.ntua.gr).

P. Rousopoulos is with the National Technical University of Athens, School of Electrical & Computer Engineering, Multimedia Technology Laboratory, Zographou Campus, 15773 Athens, Greece.

D. Dafi is with the National Technical University of Athens, School of Electrical & Computer Engineering, Multimedia Technology Laboratory, Zographou Campus, 15773 Athens, Greece, (e-mail: cpapaod@cs.ntua.gr).

M. Panagopoulos is with the National Technical University of Athens, School of Electrical & Computer Engineering, Multimedia Technology Laboratory, Zographou Campus, 15773 Athens, Greece.

V. Loumos is with the National Technical University of Athens, School of Electrical & Computer Engineering, Multimedia Technology Laboratory, Zographou Campus, 15773 Athens, Greece, (e-mail: loumos@cs.ntua.gr).

G. Theodoropoulos is with the Agricultural Univeristy of Athens, Faculty of Animal Science, Department of Anatomy and Physiology of Farm Animals, 75 Iera Odos, 11855 Athens, Greece (e-mail: gtheo@aua.gr).

Such parasite infections not only reduce productivity, but also considerable resources to be wasted on the medicinal treatment of these diseases. The correct identification of the parasite population that has infected a particular organism would allow for quick and efficient treatment of the disease, thus minimizing economic losses.

Usually, to diagnose the presence of such a parasitic infection, a coprological examination is required, where eggs produced by the strongyles are identified and quantified. However, most of the commonly encountered parasitic strongyles, such as *Haemonchus* and *Osteragia* spp., produce similarly sized and shaped eggs that are visually hard to identify at the genus level. However, the third-stage larvae, obtained after coproculture of the corresponding eggs, are sufficiently different and permit their characterization at the genus level and in some cases at the species level[1-3]. To the best of our knowledge, automated identification of third stage larvae from their digital images has not yet been achieved.

In this a paper, a novel methodology for the extraction of the unwrapped parasite outline is introduced. This methodology uses digitised parasite images, in which the motile parasite is oriented in a random fashion and may have assumed any shape. The unwrapped parasite representations may be employed for efficient automated parasite type recognition by application of fuzzy logic and/or neural networks methods.

II. Experimental Material and Setup

A. Sample Acquisition

Faecal samples obtained from naturally infected grazing sheep were collected and cultured at room temperature for 15-20 days. Larvae were recovered from the cultures using the Baermann apparatus and larvae suspensions were prepared. Drops of larva suspension were transferred onto a slide and the larvae were identified under a light microscope (OLYMPUS® BX 50 F4) using conventional identification keys[1-3]. Following identification by an expert parasitologist, three to six images of each individual motile live larva at 10x objective magnifications were recorded. A total of 255 images of 57 individual larvae in various shapes belonging to the genera *Trichostrongylus* sp. (18 individuals), *Haemonchus* sp. (6 individuals), *Oesophagostomum* sp. (11 individuals), *Cooperia* sp. (10 individuals) and *Ostertagia* sp. (12 individuals) were recorded.

B. Parasite image processing for extracting its contour

For parasite automated identification, it is necessary to obtain well-defined boundary lines of all instances of the examined deformed parasites. To achieve this, the following method is used:

- First, we have applied various image segmentation methods[4-8] in order to obtain quite clear-cut and accurate region borders of each parasite. A rather simple method that seems to work well is the one that uses each parasite's pixel intensity histogram and the lower turning point of it. All pixels with intensity lower than this turning point may be considered to belong to the parasite body. This method may generate various artifacts that may be removed by application of proper morphological filters.
- In order that the introduced methodology is applied, each contour line must have the following properties: A) each pixel must have exactly two neighboring pixels B) no isolated pixels or groups of pixels are allowed and C) three pixels must not form a compact right ($90°$) angle. Since no edge detection algorithm can generate the parasite contour in the proper form suitable software has been developed for this reason.

III. Assumptions for the Mechano-Elastic Properties of the Parasite

We will now state some concrete hypotheses concerning general elastic properties of the parasite, whose validity will be confirmed by the subsequent analysis and the experiments that will be performed.

- All parasite parts are isotropic, homogeneous and continuous.
- The parasite relative elongations are very small compared to its dimensions.
- The static equation of balance holds for the deformed element too (1st order Theory)
- The longitudinal axis of the undeformed parasite is a straight line and an axis of symmetry of it.
- The plane parasite surfaces, i.e. the cross sections, which are initially perpendicular to its symmetry axis, remain perpendicular to a proper corresponding line after the deformation.
- The cross dimensions are small compared to the parasite's length.
- The stress plane is either vertical to or includes the symmetry axis.
- The generated stresses and displacements along the parasite body are linearly related.

More specifically, general Hooke's law holds, namely the displacement tensor $\hat{\boldsymbol{\varepsilon}} = \begin{bmatrix} \varepsilon_{xx} & \tau_{xy} \\ \tau_{yx} & \varepsilon_{yy} \end{bmatrix}$ is linearly associated with the stress tensor $\hat{\boldsymbol{\sigma}} = \begin{bmatrix} \sigma_{xx} & \sigma_{xy} \\ \sigma_{yx} & \sigma_{yy} \end{bmatrix}$. Hence, the parasite body constitutive equation is $\hat{\boldsymbol{\sigma}} = \hat{\boldsymbol{A}} \cdot \hat{\boldsymbol{\varepsilon}}$, where $\hat{\boldsymbol{A}}$ is a constant matrix.

The adopted symmetry assumptions allow us to study the elastic behavior of the parasite in two dimensions. As a result, the information extracted from the parasite images may be sufficient for this study, as well as for unwrapping the parasite.

IV. Properties and Relations of the Parasite Elastic Deformation

A. The parasite element deformation

Without any loss of generality, we assume that the undeformed parasite is placed so as to have its symmetry axis parallel to the *x*-axis. Consider a differential element $AB\Gamma\Delta$ on the undeformed parasite, which, after the completion of the parasite deformation, is transformed to $A'B'\Gamma'\Delta'$. Let point *M*, which is the middle of section $A\Delta$, have coordinates $(x,0)$, while an arbitrary point *P* at section $\mathrm{A}\Delta$ is at (x, y). Moreover, we let (u, w) be the displacement of *M*, meaning that point *M'* of the deformed element has coordinates $(x + u, w)$.

Now employing assumptions of section III it results that $\overrightarrow{PP'} = \left(u - y\frac{dw}{dx}, w \right)$,

$\varepsilon_{xx} = \frac{du}{dx} - y\frac{d^2w}{dx^2}$, $\varepsilon_{yy} = 0$, $\varepsilon_{xy} = \varepsilon_{yx} = 0$ while for the stresses

$\sigma_{xx} = \mathrm{E}\varepsilon_{xx}, \sigma_{yy} = 0$, $\sigma_{xy} = \sigma_{yx} = 0$ where E is the so-called elasticity measure.

B. The Parasite neutral line

The bending moment *M* about the *x*-axis and the vertical shear force *V* on the parasite are given by $M = \int_A y\sigma_{xx} dA$ and $V = \int_{\mathrm{A}} \sigma_{xy} dA$.

After writing the equilibrium equations for the photographed parasite (fig.1) and after some straightforward calculus we obtain that $\sigma_{xx} = -yE\frac{d^2w}{dx^2}$.

Therefore, the middle of the deformed cross section suffers no stress; the curve formed by all these unstressed middle points, usually called the neutral line, has the following properties:

- It is the curve to which the symmetry axis is transformed due to the elastic deformation process.
- No stress is exerted along it.
- The neutral line and the parasite symmetry axis are of the same length.
- The undeformed cross sections initially perpendicular to the symmetry axis, remain perpendicular to the neutral line even after the parasite's deformation.

C. An important property of the deformed parasite

Let $\ell(x)$ be the upper (positive) boundary of the unstretched parasite in its 2D image; clearly $-\ell(x)$ is the lower boundary. Let AD be an arbitrary parasite cross section, intersecting the x-axis at the point $M(x,0)$ which moves to a section $A'D'$, perpendicular to the neutral line. Let also $\ell(x)$ move to the boundary curve $\vec{r}_U$ while $-\ell(x)$ to $\vec{r}_L$. If $\vec{r}_U'$ is the tangent of $\vec{r}_U$ at A' and $\vec{r}_L'$ is the tangent of $\vec{r}_L$ at D',while ϕ is the angle between $\vec{r}_U'$ and $\overrightarrow{D'A'}$ and θ the one between $\vec{r}_L'$ and $\overrightarrow{D'A'}$, then, using the previous assumptions and analysis we have demonstrated that $\phi+\theta=\pi$ (fig.1).

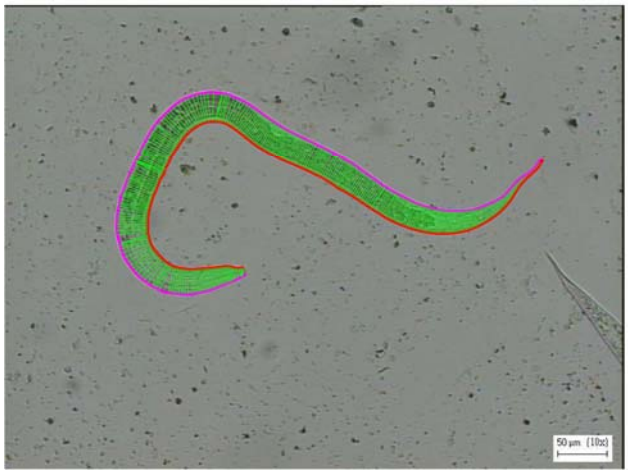

Fig.1 Approximating $\vec{r}_U$ (red) and $\vec{r}_L$ (magenta) by polynomials

V. Determining the Deformed Parasite's Neutral Line

To determine the deformed parasite neutral line we proceed as follows:

Step 1. We first extract the border of the deformed parasite from its image as described in section II. We have defined a set of curves with independent variable the contour length, to optimally fit the parasite contour. In fact we have chosen polynomials of third, fifth or seventh degree and we have employed as error criterion the quadratic norm whose minimization offered the polynomial coefficients[9]. Thus, we have achieved in approximating the parasite contour with these polynomials with an exceptionally low error (fig.2).

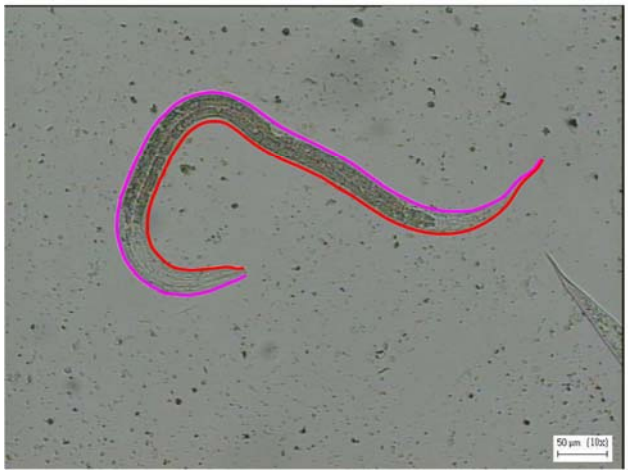

Fig.2 Determining the unstretched cross-sections of the parasite

Step 2. First, we divide the parasite border into two curves $\vec{r}_U$ and $\vec{r}_L$ (as in section IV). Next we compute all unit tangents vectors $\vec{\tau}_1^I$ at all points M_1^I of $\vec{r}_U$ as well as all unit tangent vectors $\vec{\tau}_2^J$ at all points M_2^J of $\vec{r}_L$. Thus, let $\varphi_{1,j}^I$ be the angle between $\overrightarrow{M_2^J M_1^I}$ and $\vec{\tau}_1^I$, while $\varphi_{1,j}^{II}$ be the angle between $\overrightarrow{M_2^J M_1^I}$ and $\vec{\tau}_2^J$. Then, we define the sequence $\Delta\varphi_{1,j}=\left|\varphi_{1,j}^I+\varphi_{1,j}^{II}-\pi\right|$. We define N_1^J to be that point of $\vec{r}_U$ where the minimum value of the sequence $\Delta\varphi_{1,j}$ occurs; we consequently consider the cross section joining the points M_2^J and N_1^J to be a cross section of the parasite that remains undeformed and normal to the neutral line, while the middle k^J of $\overrightarrow{M_2^J N_1^J}$ to be a point of the neutral line; clearly this procedure is repeated for all points M_2^J of the contour curve $\vec{r}_L$.

VI. Unwrapping the Parasite

We define the neutral line of the deformed parasite to be the locus of the middle points k^J determined in Section V. Clearly, the length of the neutral line remains unchanged during the various phases of the parasite deformation and it coincides with the length of the undeformed parasite's symmetry axis.

Therefore, in order to unwrap the parasite and find its undeformed shape, we proceed as follows:

1) We compute the distance of all successive middle points k^i and k^{i+1}, say δ_i.

2) Along the x-axis we form a sequence of points Λ_i of equal number with k^i, as follows: Λ_1 is placed at the axis origin; Λ_2 in the positive x-axis, so that the distance between points Λ_1 and Λ_2 is equal to the distance between middle points k^1 and k^2. We continue this process so that Λ_i and Λ_{i+1} are equidistant with k^i and k^{i+1}, until all middle points are exhausted.

3) Moving in a direction perpendicular to the x-axis at each point Λ_i we choose two points: A_i with y coordinate equal to $\lambda_i/2$, namely half the length of the cross section $\overrightarrow{M_2^i N_1^i}$ and point B_i with y coordinate $-\lambda_i/2$. We set points A_i to form the one part of the parasite, while points B_i form the other parasite part (fig.3).

Fig.3 Unwrapping 6 deformed parasite phases

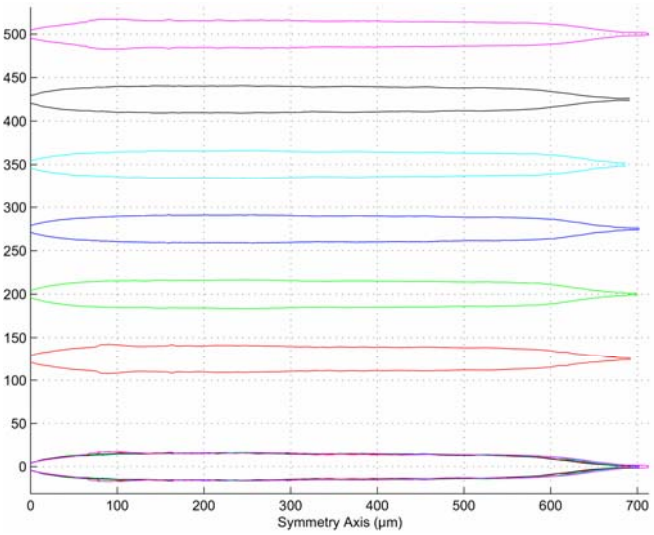

VII. Evaluation of the Results

If the assumptions made in this paper and the introduced methodology are correct, one expects that different phases of the parasite deformation will generate the same undeformed parasite version, at least with an acceptable approximation. Figure3 demonstrates that this is indeed the case. In fact, the undeformed parasite borders have a difference that might be considered negligible in respect to the parasite dimensions. We have employed five different measures to describe the differences between the shapes of the unwrapped parasite that resulted from different phases. These measures are:

1) The proportional difference in length of the unwrapped shapes.The mean value and standard deviation of this measure for the larva of figure 3 are respectively *0.82%*and *0.28%*

2) The proportional difference of the areas of the unwrapped parasites, expressed as a percentage of the average total larva area. (mean value and standard deviation of this measure *2.30%*and *1.18%).*

3) The mean value of the difference of the y-coordinates of the unwrapped shapes, expressed as a percentage of the average parasite phase diameter. (mean value and standard deviation of this measure *1.87%* and *1.06%*).

4) The proportional difference of the perimeters of the unwrapped parasites, expressed as a percentage of the average total larva perimeter. (mean value and standard deviation of this measure *0.84%* and *0.34%*).

5) The proportional difference of the maximum cross section length of the unwrapped parasites, expressed as a percentage of the average maximum cross section diameter. (mean value and standard deviation of this measure *2.63%* and *1.68%*).

Very similar measure values hold for all available parasites.

The performed experiments indicate that the average length, area, diameter and maximum cross section diameter may considerably vary between different genera. This seems to hold true for all experiments conducted so far. As these quantities are now easily and reliably quantifiable, they can be used as inputs to a pattern recognition system, which aims at identifying different parasite species. Moreover, the straightened parasite shape would be used to check for characteristics such as: roundness of the head, the length and other geometric characteristics of the tail, etc. Such a system is already under development by our team and shall be presented in detail in a future publication.

VIII. Conclusions – Further Research

In this paper, a methodology is introduced for the straightening of the contour line of a randomly oriented and shaped parasite. A digital image is used as input data, and the result is a model of the border line of the unwrapped parasite. One of the main advantages of this approach is that a large number of identification features can be extracted automatically directly from the digitised images, thus eliminating the need for user intervention. As it can be seen from the experimental results, the model contour lines obtained from different instances of the same parasite exhibit particularly low variability, which verifies the accuracy and the suitability of the chosen modelling approach. Moreover, the methodology could be used to efficiently discriminate between model lines that occurred from images of parasites belonging to different genera.

The next step in this research endeavour is to determine the parasite features, as extracted from the models obtained

from the digital images, which are most suitable for use by an automated identification system. Moreover, the straightened parasite shape would be used to check for some of the commonly used identification characteristics such as the roundness of the head or the length and other geometric characteristics of the tail. Such a system could make use of any of the currently available pattern recognition methodologies, such as neural networks, fuzzy logic, etc.

REFERENCES

[1] *Manual of Veterinary Parasitological Techniques*, Ministry of Agriculture, Fisheries and Food, Technical Bulletin No. 18, Her Majesty's Stationery Office, London, 1977

[2] L. W. McMurtry, M. J. Donaghy, A. Vlassoff and P. G. C. Douch, "Distinguishing morpho-logical features of the third larval stage of ovine Trichostrongylus spp.," *Veterinary Parasitology*, 2000, v. 90, 1-2, pp.73-81

[3] G. Theodoropoulos, V. Loumos, C. Anagnostopoulos, E. Kayafas, and B. Martinez-Gonzales, "A digital image analysis and neural network based system for identification of third-stage parasitic strongyle larvae from domestic animals," *Computer Methods and Programs in Biomedicine*, 2000, v. 62, 2, pp. 69-76

[4] Román-Roldán R., Gómez-Lopera J. F., Atae-Allah C., Martínez-Aroza J., Luque-Escamilla P. L., "A measure of quality for evaluating methods of segmentation and edge detection," *Pattern Recognition* 34, 2001,pp. 969-980.

[5] Adam, Gillian, Xiaoyi, Patrick J., Horst, Dmitry B., Kevin, David W., Andrew, Robert B., "An Experimental Comparison of Range Image Segmentation Algorithms", *IEEE Transactions on PAMI*, Vol. 18, No. 7, 1996,pp. 673-689

[6] D. Lee, S. Baek, K. Sung, "Modified k-means Algorithm for Vector Quantizer Design", *IEEE Signal Processing Letters*, Vol. 4, No. 1, 1997,pp. 2-4

[7] T.Kohonen, *Self-Organization and Associative Memory*, Berlin - Springer Verlag, 1984

[8] Panagopoulos Th., Papaodysseus C., Exarhos M., Triantafillou C., Roussopoulos G., Roussopoulos P., "Prehistoric Wall-Paintings Reconstruction Using Image Pattern Analysis And Curve Fitting," *WSEAS Transactions on Electronics* 1, no 1, 2004, pp. 108-113.

[9] C.Papaodysseus, M. Exarhos, Th. Panagopoulos, C. Triantafillou, G. Roussopoulos, Af. Pantazi, V. Loumos, D. Fragoulis, C. Doumas, "Identification of Geometrical Shapes in Paintings and its Application to Demonstrate the Foundations of Geometry in 1650 BC," *IEEE Transactions on Image Processing*, Vol. 14, No. 7, 2005.